Nano Energy 45 (2018) 210–219

Contents lists available at ScienceDirect

Nano Energy

journal homepage: www.elsevier.com/locate/nanoen

Full paper

All-in-one fiber for stretchable fiber-shaped tandem supercapacitors

Zhuanpei Wang[a], Jianli Cheng[a,*], Qun Guan[a], Hui Huang[a], Yinchuan Li[a], Jingwen Zhou[a], Wei Ni[a], Bin Wang[a,*], Sisi He[b], Huisheng Peng[b,*]

[a] Institute of Chemical Materials, China Academy of Engineering Physics, Mianyang, Sichuan 621900, China
[b] State Key Laboratory of Molecular Engineering of Polymers, Department of Macromolecular Science, and Laboratory of Advanced Materials, Fudan University, Shanghai 200438, China

ARTICLE INFO

Keywords:
All-in-one
Stretchable
Fiber-shaped supercapacitors
Tandem device
Crystalline polymer
Wearable electronics

ABSTRACT

Stretchable fiber-shaped supercapacitors (SFSSs) with high energy density and high-voltage output are becoming increasingly critical for powering wearable electronics. However, challenges still exist in the pursuit of combination of mechanical stretchability and excellent electrochemical performance due to the limitation of the fiber electrode. Here we circumvent these problems by developing a new type of "internal tandem" stretchable fiber-shaped supercapacitors based on high crystalline "all-in-one" polymer fiber. This polymer fiber has the combined properties of high conductivity, high flexibility, high specific capacitance and wide electrochemical window that can simultaneously function as electrical conductive wire and as energy storage electrode in an assembled device. The symmetric assembled tandem SFSS groups (T-SFSSs) are fabricated without the use of metal wire and additional welding connection showing tunable voltage output, tailored capacitance and outstanding stretchablility. The resulting T-SFSS assemblies consisting of 8 serially connected cells display high-voltage output of 12.8 V, ultrahigh energy density of 41.1 μW h cm^{-2} at power density of 3520 μW cm^{-2} and remarkable stretchability of up to 400% without obvious capacitance degradation. This work provides a new family of flexible fiber electrode and novel concept designs of flexible power systems that could be threaded or integrated into wearable and portable electronics.

1. Introduction

Wearable and portable electronics is emerging as a new and promising field that may revolutionize our life in the near future, and it is currently limited by finding matching power sources with sufficient energy density, good flexibility and high stretchability [1–6]. Fiber-shaped supercapacitors with advantages of being lightweight, highly flexible, soft, low-cost and wearable are considered to be one of the most promising power source candidates. Stretchable fiber-shaped supercapacitors (SFSSs) in particular can be realized by winding fiber electrodes on elastomeric substrates or by assembling fiber electrodes into a helical geometry [7,8]. For example, twisted graphene/carbon nanotube (CNT) fiber spring was used for highly stretchable supercapacitor electrodes [8–12]. A simple prestraining-and-buckling method can spin CNT sheets on an elastomeric core fiber to form either microbuckled or helically wrapped CNT structures to make highly stretchable supercapacitor electrodes [7,13–16].

Despite the progress on SFSSs, the majorities of the SFSSs to date have low stretchability and display poor electrochemical performance at high tensile strains due to the limitation of the electrode and the assembly technologies [7,17]. Since metal wires are highly conductive but are not electrochemically active for energy storage [18], most reports on SFSSs employ pseudocapacitive materials as coatings to improve the performance [19–23]. The stretchability of these electrodes is rather poor and the energy density is often limited by the coating thickness of the active material and the use of the inactive metal wire. Other fiber electrode materials may display higher energy density but their electrical conductivities are low [10,24]. On the other hand, additional metal wire interconnections are often required when electrically connecting multiple fiber supercapacitors (in series or in parallel) to satisfy the voltage or current output specifications of the intended applications, which not only added unnecessary volume, weight and cost, but also easily broke during using [10,25]. The stretchability and energy densities of the integrated device would be greatly sacrificed according to the above strategy. This approach is somehow contrary to the development of lightweight and high stretchable SFSSs [10,25]. Highly conductive and high energy storage properties fiber electrodes are therefore critical. If these fiber electrodes are realized, the development of SFSSs can avoid the need for metal wire interconnects and potentially increase the overall device

* Corresponding authors.
E-mail addresses: jianlicheng@caep.cn (J. Cheng), binwang@caep.cn (B. Wang), penghs@fudan.edu.cn (H. Peng).

https://doi.org/10.1016/j.nanoen.2017.12.054
Received 17 November 2017; Received in revised form 27 December 2017; Accepted 31 December 2017
Available online 02 January 2018

performance since unnecessary volume and weight can be minimized. Present literature shows that it is a great challenge to develop flexible, lightweight and highly conductive fiber electrodes that have high energy storage properties.

Here we demonstrate a highly stretchable tandem SFSSs prepared from an all-in-one fiber electrode that combines the function of traditional metal wire and the energy storage properties of pseudocapacitive material. This all-in-one fiber is made by wet-spinning an inherently conductive polymer, poly(3,4-ethylenedioxythiophene): poly (styrene sulfonate) (PEDOT:PSS). By applying a post-spinning treatment of sulfuric acid wash (fiber denoted as PEDOT-S:PSS), this fiber showed high tensile strength of 112.7 MPa and high electrical

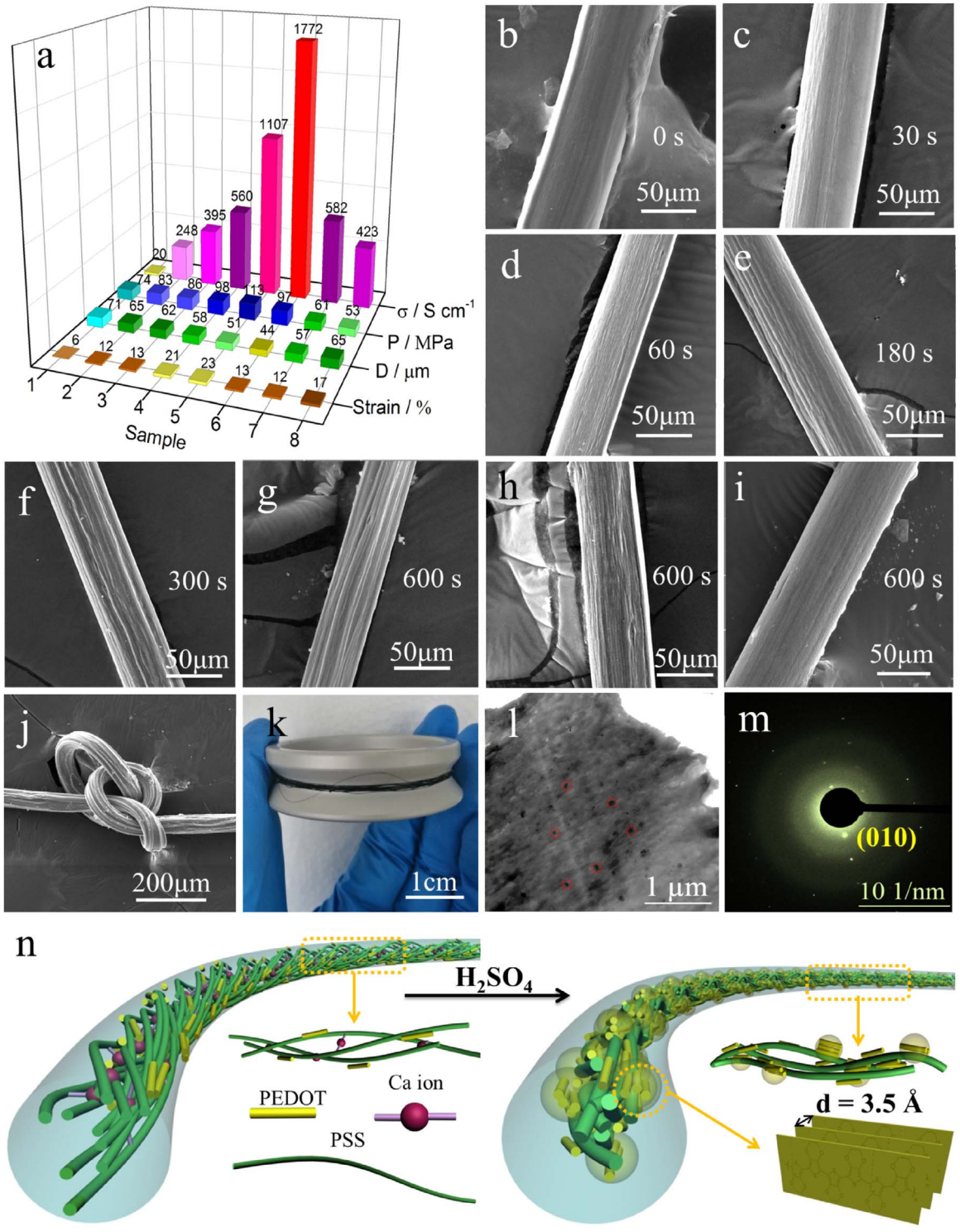

Fig. 1. (a) 3D histogram of diameter, tensile strength, tensile strain and electrical conductivity of PEDOT:PSS and PEDOT-S:PSS fibers after different treating time of sulfuric acid and solvents (Sample PEDOT-S:PSS-#1 to 8). (b-g) SEM images of PEDOT:PSS and PEDOT-S:PSS fibers after different sulfuric acid treating time (Sample PEDOT-S:PSS-#1 to 6). (h) SEM image of PEDOT-S:PSS fiber only pretreated with IPA (Sample PEDOT-S:PSS-#7). (i) SEM image of PEDOT-S:PSS fiber only pretreated with EG (Sample PEDOT-S:PSS-#8). (j) SEM image of a tied PEDOT-S:PSS fiber. k) Photograph of the continuous wet-spun PEDOT-S:PSS fiber wrapped on a PTFE reel. (l, m) TEM image and selected area electron diffraction (colored in light green) of the PEDOT-S:PSS fiber, respectively. (n) Schematic illustration to the structure re-arrangement mechanism of PEDOT-S:PSS fiber by the treatment of the sulfuric acid.

conductivity of 1771.8 S cm^{-1}. When made into symmetric FSSs, the results include a wide potential window of 1.6 V, high areal capacitance of 93.1 mF cm^{-2} (or 74.5 F cm^{-3}) at 50 μA cm^{-2} and high energy density of up to 8.3 μW h cm^{-2} (or 6.6 mW h cm^{-3}). The assembled tandem SFSS group (denoted as T-SFSS) which combines built-in stretchable conducting wires and energy storages in one device is built by connecting individual SFSSs in series without the use of additional metal wires for connection. The resulting T-SFSSs assemblies consisting of 8 serially connected cells display high-voltage output of 12.8 V and show ultrahigh energy density of 41.1 μW h cm^{-2} at power density of 3520 μW cm^{-2}, superior to that of 1-cell supercapacitor. The energy density is among the highest in the available symmetric FSSs using aqueous electrolyte. Meanwhile, the 12.8V T-SFSS assemblies possess remarkable stretchability without obvious capacitance degradation under 400% strains. This study shows great promises for the future development of integrated energy storage devices with high energy densities and high stretchability.

2. Experimental section

2.1. Materials

Clevios PH1000 (PEDOT:PSS) (1.0–1.3 wt%) was ordered from HC Starck, Inc. Ethylene glycol (EG) (AR), isopropyl alcohol (IPA) (AR), and ethanol (AR) were obtained from Sigma-Aldrich. $CaCl_2$ (AR) and concentrated H_2SO_4 (≥ 98%) were provided from Kelong Chemical Reagent Company.

2.2. Wet-spinning of PEDOT:PSS fibers

The PEDOT:PSS was concentrated to 2.0 wt% by heating at 50 °C. PEDOT:PSS fibers were prepared at room temperature using 2.0 wt% PEDOT:PSS solution by wet-spinning processes with the needle size of 25 G. The coagulating bath was ethanol/water (3/1, v/v) solution with 3 wt% $CaCl_2$. The typical extruded velocity of the solution was set at 0.5–2 mL min^{-1} using a micro syringe pump. After being dipped in the coagulation, the fibers were immersed in the EG solvent for 10 s to remove the PSS. The fibers were then washed by deionized water and subsequently the fibers were immersed in the IPA solvents for 10 s to remove the residual water. Again, the fibers were washed by deionized water and wound on a PTFE rod before drying overnight in a vacuum oven. Finally, PEDOT: PSS fibers were immersed into concentrated H_2SO_4 to remove insulate PSS. Then, the PEDOT-S:PSS fibers were sufficiently washed by deionized water and dried at 120 °C for 10 min to remove residual water. For comparison, the H_2SO_4 treated time of PEDOT-S:PSS samples labeled #1 to #8 were 0, 30, 60, 180, 300, 600, 600 and 600 s, respectively. PEDOT-S:PSS-#1 to #6 were pretreated with both EG and IPA, #7 was only pretreated with IPA, and #8 was only pretreated with EG.

2.3. Fabrication of supercapacitors

The PEDOT-S:PSS-#5 fiber with the sulfuric acid treatment by 300 s shows the best comprehensive properties. So the PEDOT-S:PSS-#5 fiber was chosen to study the structure and electrochemical performance. For FSS, two fibers were placed side by side in parallel at an interval of approximately 1 mm and covered with PVA gel electrolyte in the surface. Both ends of the fibers were fixed to the glass slide using conductive tapes. For SFSS/T-SFSS, fibers paralleled up and down were wrapped on an elastic substrate with covering PVA-H_3PO_4 gel electrolyte in the middle using a stepper motor.

2.4. Characterization and electrochemical measurement

The surface morphologies and crystal phase structures of the PEDOT:PSS and PEDOT-S:PSS fibers were characterized by scanning electron microscopy (SEM, Carl Zeiss SMT Pte Ltd., Ultra 55) and transmission electron micrographs (TEM, Zeiss Libra 200FE), operated at an acceleration voltage of 200 kV. The strain-stress curves were measured by using single fiber electronic tensile strength tester (LLY-06E). X-ray photoelectron (XPS) spectra were acquired with an Axis Ultra DLD (Shimadzu-Kratos Co.). Fourier-transform infrared (FT-IR) spectra of KBr powder pressed pellets were recorded on a Spectrum One FTIR (PerkinElmer Instrument Co.) in the range of 4000–500 cm^{-1}. Raman spectra were acquired from 400 to 3600 cm^{-1} on a Renishaw in Via Raman microscope excited by an argon ion laser beam (514.5 nm, 1.7 mW). CV and electrochemical impedance spectroscopy (EIS) measurements were carried out on a VSP-300 (Bio-Logic SAS, France) electrochemical workstation. The three electrode CV test was carried out with the Ag/AgCl as the reference electrode (3.5 mol L^{-1} KCl) and Pt plate as the counter electrode with 1 mol L^{-1} H_3PO_4 aqueous solution. EIS was recorded in a frequency range of 0.01 Hz to 100 kHz at an open-circuit voltage with an oscillation amplitude of 5 mV. The specific capacitance of the fiber was tested by the electrochemical workstation. Galvanostatic charge-discharge (GCD) measurements were conducted by using Arbin battery testing equipment (BT-2000, Arbin). The crystal phase structures were tested by X-ray diffractometer (XRD, MiniFlex 600) using Cu Kα radiation (λ = 1.5406 Å) operated at 40 kV and 40 mA.

3. Results and discussion

The wet-spinning process in preparing the PEDOT:PSS fiber is schematically shown in Fig. S1a. Briefly, the PEDOT:PSS formulation was injected into a coagulation bath of calcium chloride and washed with solvents to obtain the dried PEDOT:PSS fiber (Fig. S1b and Movie S1). This PEDOT:PSS fiber was further treated by H_2SO_4 to enhance its mechanical and electrical properties (PEDOT-S:PSS). Other solvents were also studied for comparison. Fig. 1a shows the three-dimensional (3D) histogram of diameter, tensile strength, tensile strain and electrical conductivity of different PEDOT-S:PSS fibers obtained after different treatment times. Scanning electron microscopy (SEM) analysis showed the PEDOT-S:PSS fiber became rough and wrinkled after treatment (Fig. 1b–g). Also, the fiber diameters gradually decreased to 44 μm (from 71 μm) and the electrical conductivity improved to 1771.8 S cm^{-1} (from 19.8 S cm^{-1}) with increasing treatment time (up to 600 s) (Fig. S2). The tensile strength reached the maximum value of 112.7 MPa after 300 s (Tables S1–S2, Figs. S2–S3). The resistance linearly increased with length, suggesting that the fibers are uniform and homogeneous (Fig. S4). The EG was mainly used to help the PSS move to the surface of the fiber. The IPA was used to remove the residual water of fiber and fix its fiber morphology. Therefore, the component and crystalline structure of the fiber did not change obviously after pretreatment. The tensile strength and electrical conductivity after pretreatment with solvents such as ethylene glycol (EG) and isopropyl alcohol (IPA) were relatively low (Fig. 1h–i). The PEDOT-S:PSS fiber can be spun into more than ten meters and display high flexibility that when knotted show no visible structural damage by SEM (Fig. 1j,k and Fig. S5).

Supplementary material related to this article can be found online at http://dx.doi.org/10.1016/j.nanoen.2017.12.054.

To better understand the mechanism for the improved conductivity, the microstructures of the PEDOT-S:PSS and the PEDOT:PSS fiber electrode were investigated by transmission electron microscopy (TEM) and X-ray diffraction (XRD). The PEDOT:PSS fiber exists as amorphous phase with loose and porous network structure (Fig. S6) [26–28]. The selected area electron diffraction (SAED) of the fiber cross section shows dispersion ring confirming its amorphous structure. In contrast, the PEDOT-S:PSS fiber consists of relatively ordered conductive polymer (CP) aggregates in a granular structure with spatially compact states (Fig. 1l). Furthermore, the SAED of black CP aggregates in the cross section of PEDOT-S:PSS fiber displays a crystalline structure

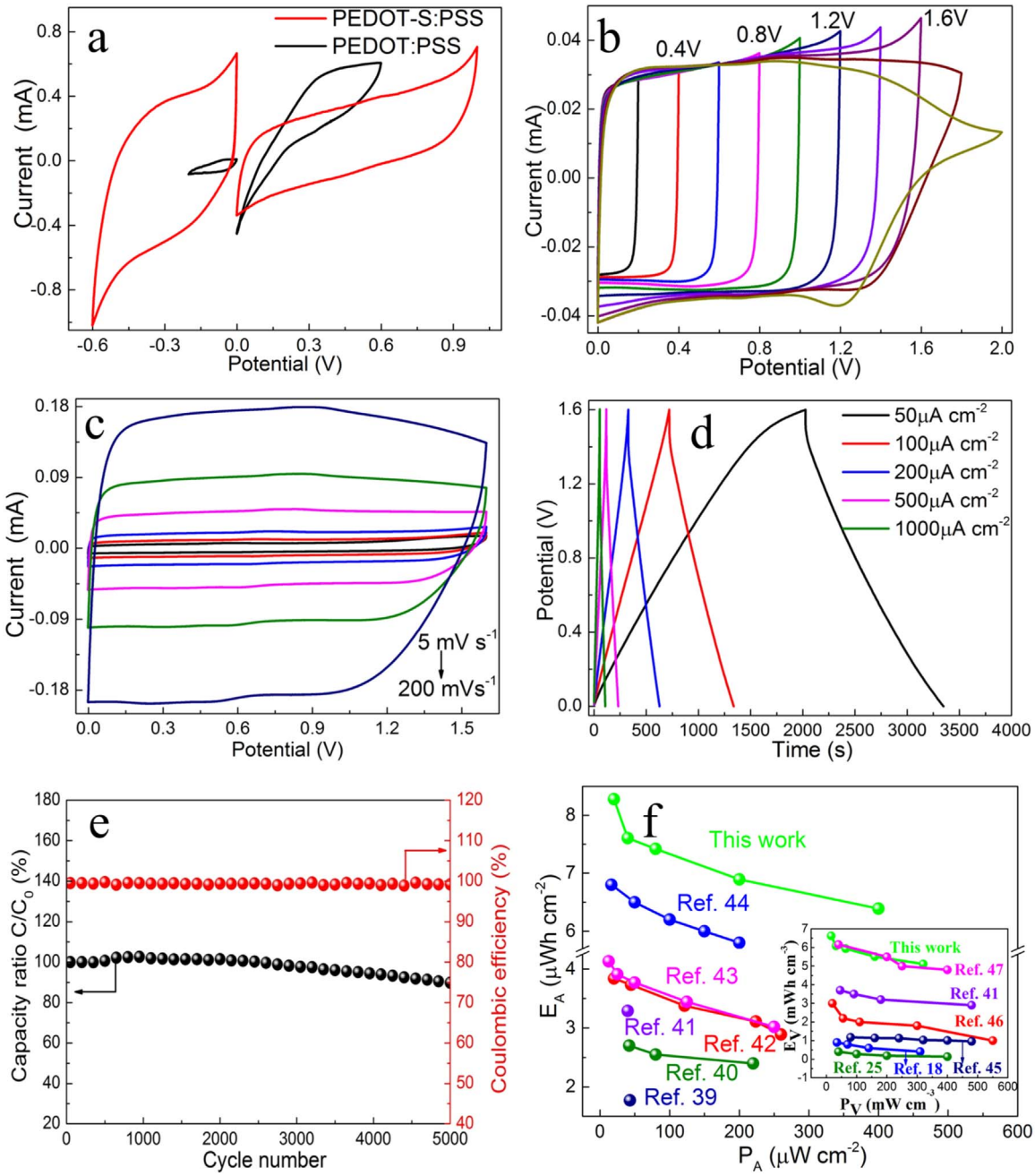

Fig. 2. Electrochemical properties of PEDOT:PSS and PEDOT-S:PSS fiber based FSSs. (a) Three-electrode cyclic voltammograms (CVs) of PEDOT:PSS and PEDOT-S:PSS based FSSs at a scan rate of 20 mV s^{-1}. (b) CV curves of PEDOT-S:PSS fiber based FSSs with different potential cutoff. (c) CV curves at different scan rates. (d) GCD curves at different current densities. (e) Cycling performance of the PEDOT-S:PSS based symmetric FSSs measured at a current density of 5000 μA cm^{-2}. (f) Comparison of Ragone plots of the PEDOT-S:PSS based symmetric FSSs with the previously reported symmetric FSSs using aqueous electrolyte (based on the two electrodes).

(Fig. 1m). The bright and sharp diffraction spot indicates a single crystalline structure with (010) orientation with a lattice spacing between the PEDOT lamellar packing chains of 3.5 Å. In comparison to PEDOT:PSS, the XRD patterns of PEDOT-S:PSS in Fig. S7 show several new diffraction peaks at 2θ = 6.4, 12.8 and 16.7° and stronger peak intensities, indicating better crystalline and more ordered structure in agreement with TEM results (Fig. 1l,m). These results show that the post-spinning treatment with sulfuric acid induced a significant structural rearrangement for the crystallization of PEDOT domains and removal of some PSS. The chemical composition of both PEDOT:PSS and PEDOT-S:PSS fibers were investigated by X-ray photoelectron spectroscopy (XPS) and Fourier transform infrared spectroscopy (FT-IR). For the PEDOT:PSS fiber, the presence of Ca 3p, 3 s, 2p and 2 s peaks at 23.5, 42.1, 346.6 and 437.8 eV, respectively, indicate the chemical bonding formation between the PEDOT:PSS and calcium originating from the calcium chloride coagulating bath (Fig. S8a). However, for the PEDOT-S:PSS fiber, these peaks are absent, suggesting the complete removal of calcium chloride by acid treatment. Furthermore, the broad band at ~ 169.3 eV attributed to O-S=O in the S 2p XPS spectra of PEDOT:PSS decreased significantly for PEDOT-S:PSS fiber, suggesting the removal of most of the PSS groups after treatment (Fig. S8b) [29]. Quantitative analysis suggests that ~ 78.2% of the PSS was removed from the PEDOT:PSS after acid treatment for 300 s. Furthermore, the main peak of the C 1s spectrum centered at ~ 284.8 eV (Fig. S8c) can be attributed to the graphitic sp^2 carbon of the PEDOT:PSS and PEDOT-S:PSS fiber [30]. It is worth noting that the shoulder peak at 286.4 eV

and the peak centered at 288.9 eV only emerge in the spectra of PEDOT-S:PSS fiber. The C 1s spectrum of the PEDOT-S:PSS fiber in Fig. S8d can be fitted to C-C bond (284.8 eV), C-O bond (286.4 eV), and the O-C=O bond (288.9 eV) [31,32] suggesting structural transformation and rearrangement of the polymer after treatment.

The FT-IR spectrum of the PEDOT:PSS fiber shows several characteristic bands at 1520, 1393, 1323 and 1194 cm^{-1} (Fig. S9), which can be attributed to the C=C stretching of benzene rings and the C-C stretching of backbone and sulfonic group of PSS, respectively [33,34]. The sharp band at 1090 cm^{-1} has been ascribed to the p-doped PEDOT in literature [35]. Furthermore, all of the characteristic bands that correspond to PSS decreased significantly for the PEDOT-S:PSS fiber, indicating the removal of most PSS after treatment, which is consistent with the XPS results. The Raman spectra in Fig. S10 show the five characteristic peaks of PEDOT at 1564, 1514, 1434, 1361 and 1266 cm^{-1}, which could be assigned to the C-C anti-symmetric stretching, C=C asymmetric stretching, C=C symmetric stretching, C-C single bond stretching and C-C inter-ring stretching of PEDOT [31,36]. The five peaks gradually increased in intensity and the peak widths at half-maximum gradually decreased for the fibers obtained at different acid treatment times, suggesting the increased degree of crystallinity of PEDOT with prolonged treatment time [37].

The formation of ordered crystalline structure in the CPs is known to facilitate efficient charge transport between intramolecular chain and/or intermolecular chain and results in enhanced conductivity and electrochemical performance [27,38]. From the above results, we propose that the structural changes in the PEDOT-S:PSS fiber occur as illustrated in Fig. 1n. During the coagulation of PEDOT:PSS formulation in the $CaCl_2$ coagulation bath, calcium ions crosslink some of the negatively polymer chains but majority of the PSS are washed away during acid treatment. This removal of PSS allows for the rearrangement of PEDOT chains and leads to a densely packed structure of highly ordered crystalline aggregates due to the strong π-π stacking of the PEDOT backbone. These structural changes dramatically improve the crystallinity, morphology and charge carrier characteristics of the PEDOT-S:PSS fiber as reflected in the enhanced electrical conductivity and tensile strength.

To investigate the electrochemical properties of the PEDOT:PSS and PEDOT-S:PSS fiber, symmetric fiber-shaped supercapacitors (FSSs) were assembled using polyvinyl alcohol (PVA) and phosphoric acid (H_3PO_4) gel electrolyte. Fig. 2a compares the cyclic voltammograms (CV) of the PEDOT:PSS and PEDOT-S:PSS at 20 mV s^{-1}. Previous results showed that the presence of insulating PSS and Ca^{2+} in the PEDOT:PSS strongly decrease the charge transport [35]. In the case of device made from PEDOT:PSS fibers, the potential window was found to be 0.8 V based on the stable CV response between 0–0.6 V (as positive electrodes) and between −0.2–0 V (as negative electrodes). In contrast, the potential window of the device made from PEDOT-S:PSS fiber was 1.6 V from stable responses at 0–1.0 V and −0.6–0 V, as positive and negative electrodes, respectively. The CV curves of the PEDOT-S:PSS fiber based FSSs show rectangular shape with fast current response to voltage reversal, reflecting good electrochemical performance of the device (Fig. S11). At 5 mV s^{-1}, the areal capacitance of the PEDOT-S:PSS fiber (91.1 mF cm^{-2}) is approximately two times that of PEDOT:PSS fiber (55.7 mF cm^{-2}). For the device with PEDOT-S:PSS fiber, the rectangular shapes of the CV curves were maintained up to 200 mV s^{-1} (Fig. 2c), indicating outstanding high rate capabilities. The assembled symmetric FSSs based on PEDOT-S:PSS fiber showed stable CV response at different potential windows (Fig. 2b). By extending the potential window from 0.8 to 1.6 V and increasing the specific capacitance, the energy density of the device improved by 670%. The results of galvanostatic charge-discharge (GCD) tests are consistent with the CV tests. At a current density of 500 μA cm^{-2}, the device maintained a symmetric GCD curve up to 1.6 V as shown in Fig. S12. Accordingly, the energy densities of the devices made from PEDOT-S:PSS fibers improved from 2.8 to 8.3 μW h cm^{-2} when the potential window was increased from 1.0 V to1.6 V.

GCD tests were conducted in the potential range of 0–1.6 V with current densities from 50 to 1000 μA cm^{-2} (Fig. 2d). The GCD curves showed triangular shapes with very low iR drops. A linear relationship between the potential and time was observed when the current density was increased from 50 to 1000 μA cm^{-2} validating the efficient capacitance behavior and charge propagation between the two fiber electrodes. At a current density of 50 μA cm^{-2}, the areal capacitance of PEDOT-S:PSS fibers reached 93.1 mF cm^{-2} (corresponding to a volumetric capacitance of 74.5 F cm^{-3} and a mass capacitance of 69.63 F g^{-1}). The excellent rate capability is demonstrated by maintaining very high areal capacitance of 77.5 and 71.9 mF cm^{-2} even at current densities of 500 and 1000 μA cm^{-2}, respectively.

The cycling stability of the symmetric FSS device with PEDOT-S:PSS fiber was also investigated using GCD (Fig. 2e and Fig. S13). After 5000 cycles at 5000 μA cm^{-2}, the specific capacitance retention was ~ 89% and the Coulombic efficiency was nearly 100%. The morphology (Fig. S14a, b) and the Raman spectra (Fig. S15) of the PEDOT-S:PSS fiber did not show distinct changes before and after cycling, revealing structural stability. In addition, the TEM images and SAED patterns also indicated that the single crystalline structure was maintained after cycling, further confirming its stability (Fig. S16).

The energy and power densities are important for practical applications. Fig. 2f compares the Ragone plot of PEDOT-S:PSS based symmetric FSSs with that of the previously reported symmetric FSSs that use aqueous gel electrolyte. Here, the asymmetric FSSs and the symmetric FSSs using organic electrolyte are excluded to avoid confusion when comparing electrode materials. The PEDOT-S:PSS based symmetric FSSs show a high areal energy density of 8.3 μW h cm^{-2} (based on two fiber electrodes) with a maximum power density of 400 μW cm^{-2}. This areal energy density of 8.3 μW h cm^{-2} is much higher than those of other aqueous symmetric FSSs based on OMC/CNT (1.77 μW h cm^{-2} and 43 μW cm^{-2}) [39], pen ink Au/plastic wire (2.7 μW h cm^{-2} and 220 μW cm^{-2}) [40], SWNT@C (3.29 μW h cm^{-2} and 3360 μW cm^{-2}) [41], RGO/CNT fiber (3.84 μW h cm^{-2} and 260 μW cm^{-2}) [42], PEDOT:PSS fiber (4.13 μW h cm^{-2} and 250 μW cm^{-2}) [43], and graphene/PEDOT fiber (6.80 μW h cm^{-2} and 200 μW cm^{-2}) [44]. Moreover, it is worth noting that the volumetric energy density of the PEDOT-S:PSS based symmetric FSSs can reach 6.6 mW h cm^{-3} (based on two fiber electrodes) with a maximum power density of 320 mW cm^{-3} (inset of Fig. 2f). The volumetric energy density of 6.6 mW h cm^{-3} exceeds those of Ag-nanowire/PEDOT: PSS nanopillar/MnO_2 (0.406 mW h cm^{-3} and 400 mW cm^{-3}) [25], CuO@AuPd@MnO_2 fiber (0.9 mW h cm^{-3} and 310 mW cm^{-3}) [18], CNT/MoS_2 composites (1.18 mW h cm^{-3} and 480 mW cm^{-3}) [45], CNT/MoS_2 hybrid fiber (3.0 mW h cm^{-3} and 550 mW cm^{-3}) [46], SWNT@C yarn (3.7 mW h cm^{-3} and 3840 mW cm^{-3}) [41], PPy/MnO_2/carbon fiber (6.16 mW h cm^{-3} and 400 mW cm^{-3}) [47], and comparable to that of 4 V-500 μA h thin-film lithium batteries (0.3–10 mW h cm^{-3}).

Electrochemical impedance spectroscopy (EIS) measurements were also conducted to further understand the electrochemical behavior of the fiber electrodes. Fig. S17 shows the Nyquist plots of PEDOT-S:PSS and PEDOT:PSS fiber. The vertical straight line in the low frequency demonstrates excellent capacitive characteristics of the fiber electrodes. The equivalent series resistance (ESR), which comes from the internal resistance of electrodes and the Ohmic resistance of electrolyte, was obtained from the real axis intercept of the Nyquist plot in the high frequency region. The PEDOT-S:PSS fiber exhibits a significantly lower ESR (106.9 Ω) than PEDOT:PSS fiber (4084.4 Ω, Fig. S17 inset), consistent with the electrical conductivity results. The efficient electron transport and faster ion diffusion ability are also reflected in the superior electrochemical performance of the PEDOT-S:PSS electrode.

To demonstrate flexibility and stretchability of the PEDOT-S:PSS fiber based single SFSS for practical use in wearable electronics, the electrochemical performance under different degrees of bending and stretching were investigated. As shown in Fig. 3a, b, the CV curves remained almost unchanged when the devices were bent up to 180° for

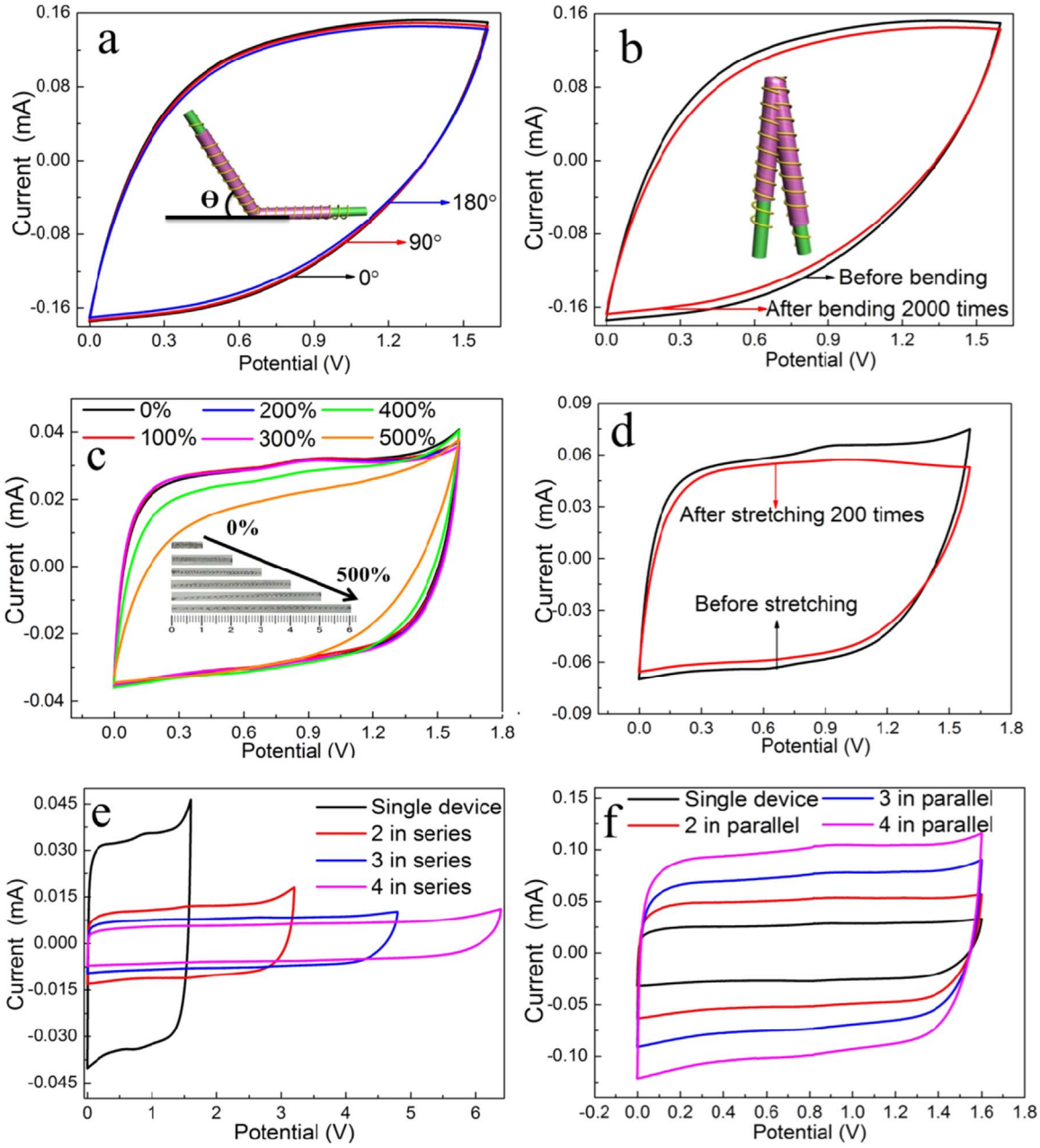

Fig. 3. (a) CV curves of PEDOT-S:PSS based SFSSs bent at increasing angles at a scan rate of 20 mV s^{-1}, and the inset is the illustration of PEDOT-S:PSS based SFSSs at different bending angles. (b) CV curves of PEDOT-S:PSS based SFSSs bent after 2000 times at a scan rate of 20 mV s^{-1}, and the inset is the illustration of PEDOT-S:PSS based SFSSs at a bending angle of 180°. (c) CV curves of PEDOT-S:PSS based SFSSs under increasing strains at a scan rate of 20 mV s^{-1}, and the insets are the photographs of PEDOT-S:PSS based SFSSs under increasing strains from 0% to 500%. (d) CV curves of PEDOT-S:PSS based SFSSs before and after stretching by 300% for 200 times. (e) CV curves of one, two, three and four series-connected PEDOT-S:PSS based FSSs at a scan rate of 20 mV s^{-1}. (f) CV curves of one, two, three and four parallel-connected PEDOT-S:PSS based FSSs at a scan rate of 20 mV s^{-1}.

2000 times. Meanwhile, the electrochemical performances were also maintained even after being stretched to 500%. The specific capacitances of the FSSs could retain 94% of their original specific capacitance even after 200 times of 300% stretching (Fig. 3c, d). Furthermore, by optimizing the electrode structure, the single supercapacitor could even be stretched up to 800% (Fig. S18a). The CV curves of the supercapacitor did not show obviously change under different stretching from 0% to 800% (Fig. S18b), demonstrating excellent flexibility. The reversibility could be further optimized by using different components gel electrolytes (Fig. S18c). Fig. 3e shows the CV curves for FSS assemblies that are electrically connected in series, where each device assembly showed increasing potential windows of 1.6, 3.2, 4.8 and 6.4 V for the respective assembly that contain one, two, three and four FSSs. The normalized capacitance of each series-connected FSS proportionately decreased with the FSS number. When four FSSs were connected in parallel, the output current was approximately four times than that of a single FSS device demonstrating a linear increase between the output capacitance and the number of supercapacitors (Fig. 3f). These results demonstrate that the PEDOT-S:PSS fiber based FSSs could be effectively designed for a variety of wearable applications.

The assembled tandem SFSS group (denoted as T-SFSS) which combines stretchable conducting wire and energy storage in one device is further built by connecting individual SFSSs electrically in series without the use of additional metal wires for connection. This means that in the T-SFSS device, each SFSS was seamlessly, electrically connected in series by using the all-in-one fibers serve as both the conductive wire for electrical connection and the active electrode material for energy storage, as schematically illustrated in Fig. 4a. To investigate the influence of charging process while the

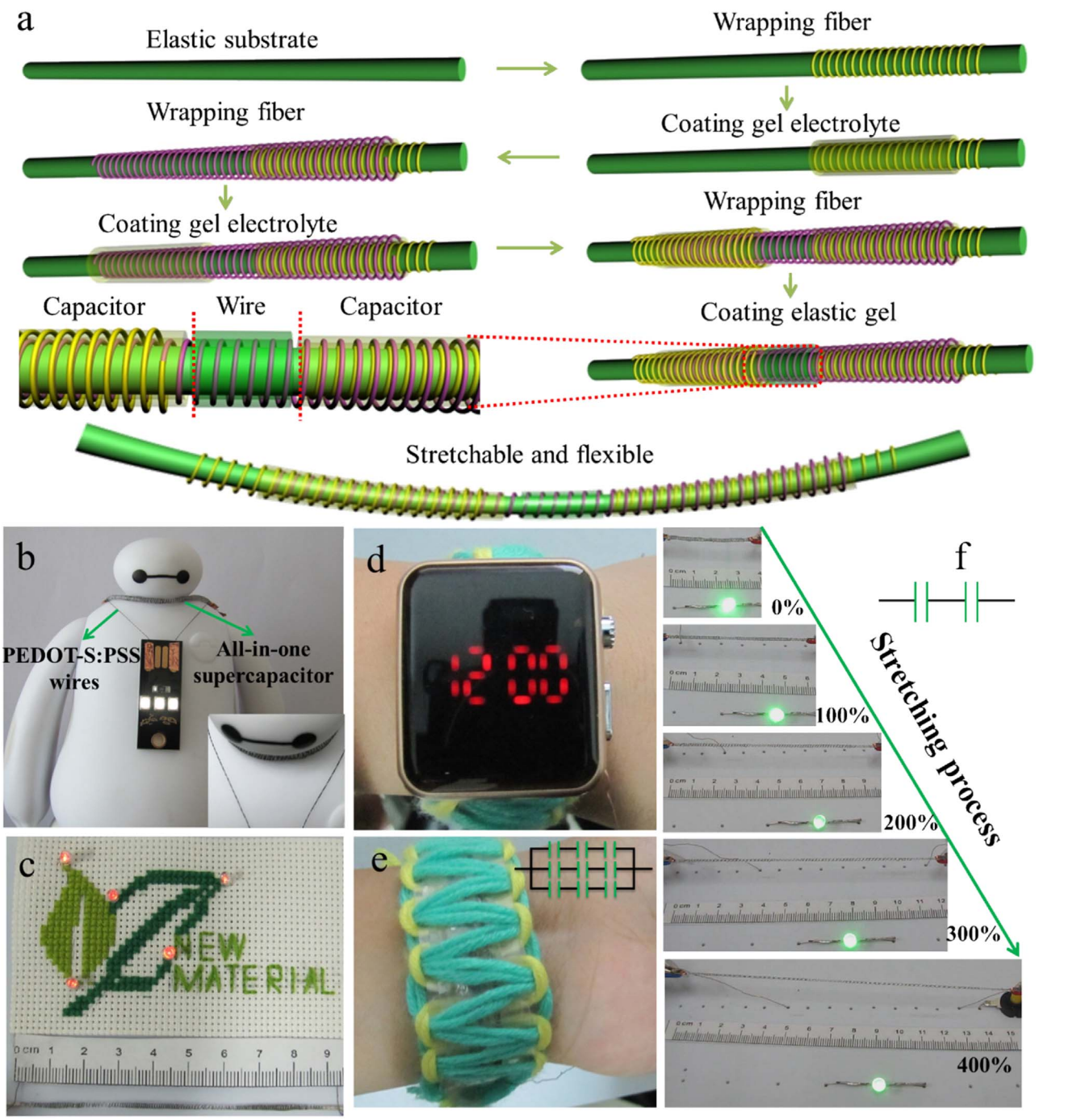

Fig. 4. (a) Schematic illustration to the fabrication of PEDOT-S:PSS based assembled T-SFSSs in series. (b) Photograph of T-SFSSs to lighten up a commercial USB light. The inset is the photograph showing the USB light connected with the T-SFSSs by two twisted PEDOT-S:PSS fibers. (c) Photograph of the T-SFSSs consisting of three series-connected SFSSs to lighten up a logo abbreviation with five light-emitting diodes (LEDs). (d, e) Photographs of a commercial digital watch powered by three connected T-SFSSs woven into a fabric. Each consisted of three PEDOT-S:PSS fiber based series-connected T-SFSSs. (f) Photograph of T-SFSSs consisting of two series-connected SFSSs to lighten up a green LED under increasing strains from 0% to 400%.

PEDOT-S:PSS fibers are simultaneously used as the built-in conducting wire and as the energy storage electrodes, we measured the electrical resistance of the fibers using a two-probe method. It was found that the electrical resistance from the current-potential (I-V) curves before and after charging only showed minor fluctuations (Fig. S19) demonstrating its suitability for the proposed two functions in one device. As demonstrations, the T-SFSSs consisting of 2 series-connected SFSSs were used to power a commercial USB light that operated at a minimum voltage of 2.5 V (Fig. 4b). In Fig. 4c and Fig. S20, the T-SFSSs consisting of 3 series-connected SFSSs could provide an output voltage of 4.5 V, which can easily lighten up a logo abbreviation with five light-emitting diodes (LEDs). The potential and capacitance of T-SFSSs can be easily turned by serial and parallel assemblies. Furthermore, 3 parallel-connected T-SFSSs were woven into a fabric textile to power a commercial digital watch (3.0 V, 100 mW, Fig. 4d, e). Also, a 3.2 V T-SFSS based on the all-in-one fibers was designed to withstand a stretching strain of up to 400% (Fig. 4f). Compared with other group supercapacitors such as those connected by spring-like metal wires (Fig. S21), the T-SFSSs reported here demonstrate improved stretchability without the need for additional electrical connections with metal wires (usually welded or glued) that can break during deformation. To further demonstrate the

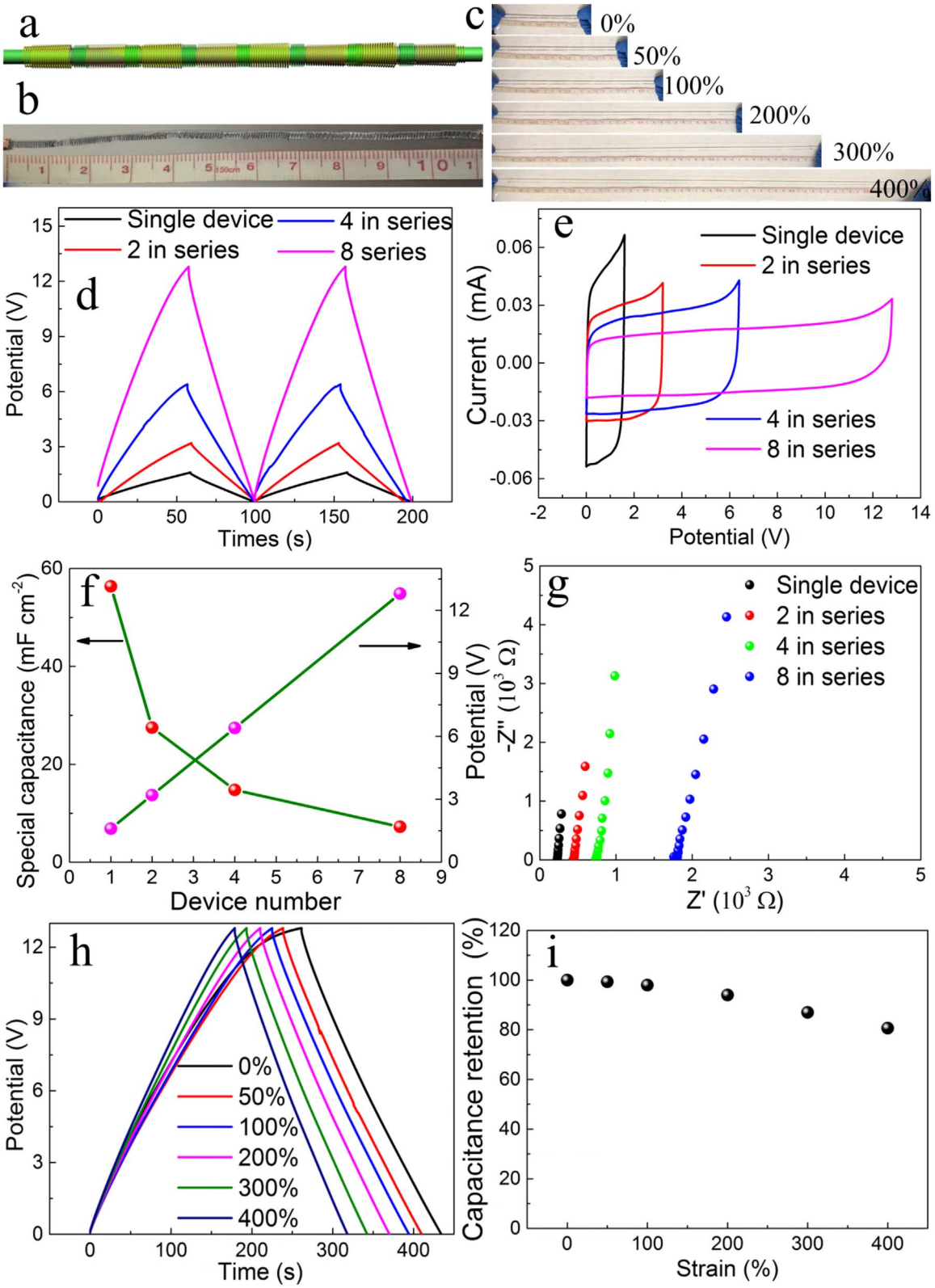

Fig. 5. Electrochemical performance of T-SFSSs. (a) Schematic illustration and (b) Photograph of T-SFSSs consisting of 8 series-connected SFSSs. (c) Photograph of T-SFSSs consisting of 8 series-connected SFSSs under increasing strains from 0% to 400%. (d) The GCD profiles of the T-SFSSs with 1, 2, 4, 8 series-connected SFSS cells measured at a current density of 1 mA cm^{-2}. (e) CV curves of T-SFSSs with the increasing cells obtained at a scan rate of 50 mV s^{-1}. (f) Plots of voltage output and capacitance versus serial device number. (g) EIS curves of T-SFSSs consisting of 1, 2, 4, 8 series-connected cells. (h) GCD profiles of T-SFSSs consisting of 8 series-connected SFSSs under increasing strains from 0% to 400%. (i) Changes in the normalized capacitance as a function of the tensile strain based on the GCD curves.

advantages of the internal tandem structure, T-SFSSs consisting of 8 cells were tested and discovered (Fig. 5a). As demonstrated in Fig. 5b and c, the T-SFSSs with a voltage of 12.8 V and a length of 11 centimetres could be stretched up to 400%. Fig. 5d shows the GCD profiles of the T-SFSSs with 1, 2, 4 and 8 serially connected SFSSs. As a result, T-SFSSs showed a stepwise linear increase in the working voltage from 1.6 to 12.8 V by increasing the number of serial cells. Meanwhile, the corresponding capacitance monotonically decreased (Fig. 5f, Table S3). Consistent with the GCD, the CV curves of T-SFSSs displayed a nearly identical rectangular shape tested at 50 mV s^{-1}, with the linear increase of the working voltage versus cell numbers and the responding current decreased correspondingly (Fig. 5e, f).

The EIS curves of T-SFSSs are shown in Fig. 5g. The corresponding ESR of T-SFSSs for 1, 2, 4 and 8 series-connected cells were about 227.3, 435.6, 739.7 and 1757.8 Ω, respectively, which are approximately equal to the theoretical values (Table S4). The ESR values of T-SFSSs were linearly increased with the integrated cell numbers and the ESR value of T-SFSSs with 8 cells was approximately eight times that of single SFSS, demonstrating the excellent uniformity of the integrated device and high electrical conductivity of the all-in-one polymer fiber.

Energy and power densities are important parameters in the supercapacitor energy storage applications. It is pointed out that although the overall capacitance of the T-SFSSs was nearly inversely proportional to the cell number, the energy densities of the integrated device were increased significantly according to the equation of $E = 0.5 \times C \times U^2$ [48]. As shown in Table S3, our integrated 8-cell T-SFSSs show very high energy density of 41.1 μW h cm^{-2} at power density of 3520 μW cm^{-2}, superior to that of 1-cell supercapacitor with energy density of 5.0 μW h cm^{-2} at power density of 440 μW cm^{-2}. Furthermore, by combination of stretchable charge conduction and energy storage in one electrode, the 12.8 V T-SFSS groups containing 8 cells could also be cycled under stains. As shown in Fig. 5h–i, the GCD curves remained mostly unchanged when the strains increased and more than 80% of the capacitance was maintained up to a strain of 400%. Therefore, by using the all-in-one fiber electrode, the T-SFSSs with remarkable properties including the high stretchability, high output voltages and high energy densities could be achieved. The comparisons between the PEDOT-S:PSS fiber based SFSSs with the previously reported stretchable supercapacitors are summarized in Table S5. To the best of our knowledge, this is the highest stretchability achieved so far for stretchable tandem fiber-shaped supercapacitors.

4. Conclusions

In summary, we demonstrated a new fiber electrode with outstanding properties such as high electrical conductivity (1771.8 S cm^{-1}), high tensile strength (112.7 MPa) and outstanding electrochemical properties. This fiber was used to construct novel stretchable fiber-shaped supercapacitors with wide electrochemical window (1.6 V), high areal and volumetric energy densities (8.3 μW h cm^{-2} and 6.6 mW h cm^{-3}, respectively), high areal and volumetric power densities (400 μW cm^{-2} and 320 mW cm^{-3}, respectively) and stable cycling performance (89% capacitance retention after 5000 cycles). The high conductivity of this fiber also enabled the simple fabrication of stretchable tandem supercapacitors group by electrically connecting several SFSSs in series without using metal wire interconnects. The resulting T-SFSS groups consisting of 8 serially connected cells displayed high-voltage output of 12.8 V, ultrahigh energy density of 41.1 μW h cm^{-2} at power density of 3520 μW cm^{-2} and remarkable stretchability of up to 400% without obvious capacitance degradation. These outstanding performance and novel design represent a highly promising power system for wearable and portable electronics.

Acknowledgments

This work was supported by the National Natural Science Foundation of China (Nos. 51741305, 21501160 and 21401177), the Science Foundation for Distinguished Young Scholars of Sichuan Province (2016JQ0025 and 2017JQ0036), the “QianYingBaiTuan” Plan of China Mianyang Science City, the Science Foundation of Institute of Chemical Materials (No. 011100301) and the “1000plan” from the Chinese Government.

Appendix A. Supporting information

Supplementary data associated with this article can be found in the online version at http://dx.doi.org/10.1016/j.nanoen.2017.12.054

References

[1] J. Bae, M.K. Song, Y.J. Park, J.M. Kim, M. Liu, Z.L. Wang, Angew. Chem. Int. Ed. 50 (2011) 1683–1687.
[2] X. Wang, K. Jiang, G. Shen, Mater. Today 18 (2015) 265–272.
[3] W. Weng, S. He, X. Sun, H. Peng, Angew. Chem. Int. Ed. 55 (2016) 6140–6169.
[4] W. Zeng, L. Shu, Q. Li, S. Chen, F. Wang, X.M. Tao, Adv. Mater. 26 (2014) 5310–5336.
[5] M. Zhu, Y. Huang, Y. Huang, H. Li, Z. Wang, Z. Pei, Q. Xue, H. Geng, C. Zhi, Adv. Mater. 29 (2017) 1605137.
[6] Y. Huang, M. Zhu, Y. Huang, Z. Pei, H. Li, Z. Wang, Q. Xue, C. Zhi, Adv. Mater. 28 (2016) 8344–8364.
[7] Z. Yang, J. Deng, X. Chen, J. Ren, H. Peng, Angew. Chem. Int. Ed. 52 (2013) 13453–13457.
[8] Y. Shang, C. Wang, X. He, J. Li, Q. Peng, E. Shi, R. Wang, S. Du, A. Cao, Y. Li, Nano Energy 12 (2015) 401–409.
[9] S. Wang, N. Liu, J. Su, L. Li, F. Long, Z. Zou, X. Jiang, Y. Gao, ACS Nano 11 (2017) 2066–2074.
[10] Y. Meng, Y. Zhao, C. Hu, H. Cheng, Y. Hu, Z. Zhang, G. Shi, L. Qu, Adv. Mater. 25 (2013) 2326–2331.
[11] H. Wang, C. Wang, M. Jian, Q. Wang, K. Xia, Z. Yin, M. Zhang, X. Liang, Y. Zhang, Nano Res. (2017), http://dx.doi.org/10.1007/s12274-017-1782-1.
[12] J. Yu, W. Lu, J.P. Smith, K.S. Booksh, L. Meng, Y. Huang, Q. Li, J.-H. Byun, Y. Oh, Y. Yan, T.-W. Chou, Adv. Energy Mater 7 (2017) 1600976.
[13] M. Li, M. Zu, J. Yu, H. Cheng, Q. Li, Small 13 (2017) 1602994.
[14] T. Chen, R. Hao, H. Peng, L. Dai, Angew. Chem. Int. Ed. 54 (2015) 618–622.
[15] J. Sun, Y. Huang, C. Fu, Z. Wang, Y. Huang, M. Zhu, C. Zhi, H. Hu, Nano Energy 27 (2016) 230–237.
[16] Z. Zhang, J. Deng, X. Li, Z. Yang, S. He, X. Chen, G. Guan, J. Ren, H. Peng, Adv. Mater. 27 (2015) 356–362.
[17] X. Chen, H. Lin, P. Chen, G. Guan, J. Deng, H. Peng, Adv. Mater. 26 (2014) 4444–4449.
[18] Z. Yu, J. Thomas, Adv. Mater. 26 (2014) 4279–4285.
[19] Q. Ke, C. Guan, X. Zhang, M. Zheng, Y.W. Zhang, Y. Cai, H. Zhang, J. Wang, Adv. Mater. 29 (2017) 1604164.
[20] Z.S. Wu, Y. Zheng, S. Zheng, S. Wang, C. Sun, K. Parvez, T. Ikeda, X. Bao, K. Mullen, X. Feng, Adv. Mater. 29 (2017) 1602960.
[21] B. Anothumakkool, R. Soni, S.N. Bhange, S. Kurungot, Energy Environ. Sci. 8 (2015) 1339–1347.
[22] C. Yin, C. Yang, M. Jiang, C. Deng, L. Yang, J. Li, D. Qian, ACS Appl. Mater. Interfaces 8 (2016) 2741–2752.
[23] R. Liu, J. Duay, S.B. Lee, ACS Nano 4 (2010) 4299–4307.
[24] B. Yao, H. Wang, Q. Zhou, M. Wu, M. Zhang, C. Li, G. Shi, Adv. Mater. (2017) 1700974.
[25] Z. Yu, C. Li, D. Abbitt, J. Thomas, J. Mater. Chem. A 2 (2014) 10923–10929.
[26] R. Jalili, J.M. Razal, P.C. Innis, G.G. Wallace, Adv. Funct. Mater. 21 (2011) 3363–3370.
[27] N. Kim, S. Kee, S.H. Lee, B.H. Lee, Y.H. Kahng, Y.R. Jo, B.J. Kim, K. Lee, Adv. Mater. 26 (2014) 2268–2272.
[28] J. Rivnay, S. Inal, B.A. Collins, M. Sessolo, E. Stavrinidou, X. Strakosas, C. Tassone, D.M. Delongchamp, G.G. Malliaras, Nat. Commun. 7 (2016) 11287.
[29] H. Yan, H. Okuzaki, Synth. Met. 159 (2009) 2225–2228.
[30] S. Cho, M. Kim, J. Jang, ACS Appl. Mater. Interfaces 7 (2015) 10213–10227.
[31] D. Yoo, J. Kim, J.H. Kim, Nano Res. 7 (2014) 717–730.
[32] D. Sun, L. Jin, Y. Chen, J.-R. Zhang, J.-J. Zhu, ChemPlusChem 78 (2013) 227–234.
[33] Y. Li, G. Ren, Z. Zhang, C. Teng, Y. Wu, X. Lu, Y. Zhu, L. Jiang, J. Mater. Chem. A 4 (2016) 17324–17332.
[34] N.K. Sadanandhan, S.J. Devaki, R.K. Narayanan, M. Cheriyathuchenaaramvalli, ACS Appl. Mater. Interfaces 7 (2015) 18028–18037.
[35] D.K. Bhat, M. Selva Kumar, J. Mater. Sci. 42 (2007) 8158–8162.
[36] H.J. Lee, G. Anoop, H.J. Lee, C. Kim, J.-W. Park, J. Choi, H. Kim, Y.-J. Kim, E. Lee, S.-G. Lee, Y.-M. Kim, J.-H. Lee, J.Y. Jo, Energy Environ. Sci. 9 (2016) 2806–2811.
[37] T. Deschaines, J. Hodkiewicz, P. Henson, T. Scientific, Spectroscopy, Madison, WI, USA, February 1, 2009.
[38] S. Kee, N. Kim, B.S. Kim, S. Park, Y.H. Jang, S.H. Lee, J. Kim, J. Kim, S. Kwon, K. Lee, Adv. Mater. 28 (2016) 8625–8631.
[39] J. Ren, W. Bai, G. Guan, Y. Zhang, H. Peng, Adv. Mater. 25 (2013) 5965–5970.
[40] Y. Fu, X. Cai, H. Wu, Z. Lv, S. Hou, M. Peng, X. Yu, D. Zou, Adv. Mater. 24 (2012) 5713–5718.
[41] Q. Meng, H. Wu, Y. Meng, K. Xie, Z. Wei, Z. Guo, Adv. Mater. 26 (2014) 4100–4106.
[42] L. Kou, T. Huang, B. Zheng, Y. Han, X. Zhao, K. Gopalsamy, H. Sun, C. Gao, Nat. Commun. 5 (2014) 3754.
[43] D. Yuan, B. Li, J. Cheng, Q. Guan, Z. Wang, W. Ni, C. Li, H. Liu, B. Wang, J. Mater. Chem. A 4 (2016) 11616–11624.
[44] G. Qu, J. Cheng, X. Li, D. Yuan, P. Chen, X. Chen, B. Wang, H. Peng, Adv. Mater. 28 (2016) 3646–3652.

[45] T. Lv, Y. Yao, N. Li, T. Chen, Angew. Chem. Int. Ed. 55 (2016) 9191–9195.
[46] Y. Luo, Y. Zhang, Y. Zhao, X. Fang, J. Ren, W. Weng, Y. Jiang, H. Sun, B. Wang, X. Cheng, H. Peng, J. Mater. Chem. A 3 (2015) 17553–17557.
[47] J. Tao, N. Liu, W. Ma, L. Ding, L. Li, J. Su, Y. Gao, Sci. Rep. 3 (2013) 2286.
[48] W. Chen, C. Xia, H.N. Alshareef, Nano Energy 15 (2015) 1–8.

Zhuanpei Wang received her M.S. degree in Materials Science and Engineering at Southwest University of Science and Technology in 2015. She is currently pursuing his Ph.D. degree under the supervision of Prof. Hui Huang and Bin Wang at Institute of Chemical Materials, China Academy of Engineering Physics since 2015. She has been focusing her research attention on electrochemical energy conversion and storage devices, including wearable supercapacitors, Lithium batteries and dye-sensitized solar cells.

Jianli Cheng received her Ph.D. degree from Fudan University in 2009. After working at Lawrence Berkeley National Laboratory (Berkeley, USA), she is now an associate professor at China Academy of Engineering Physics. Her research focuses on fabrication and application of new materials for flexible energy storage/conversion, particularly in batteries and supercapacitors.

Quan Guan received her master degree in Chemical Engineering from Southwest University of Science and Technology, Mianyang, China, in 2015. She is currently working as assistant research at Institute of Chemical Materials, China Academy of Engineering Physics. Her current research interests are synthesis of carbon materials and their applications in supercapacitors and Lithium batteries.

Hui Huang received his B.S. degree from North China Institute of Technology in 1982, his master degree from Beijing Institute of Technology in 2002 and Ph.D. degree from Nanjing University of Science and Technology in 2009. He joined Institute of Chemical Materials, China Academy of Engineering Physics as a researcher in 1982. He is currently a PhD supervisor at China Academy of Engineering Physics and Nanjing University of Science and Technology. His research interests focus on sustainable energy applications including supercapacitors and fuel cells.

Yinchuan Li received his M.S. in applied chemistry from Southwest University of Science and Technology in 2014 and joined Prof. Bin Wang's group in 2016. Now he works as a research assistant in Institute of Chemical Materials, CAEP. His current research focuses on developing fibrous flexible electrode materials for novel rechargeable batteries.

Jingwen Zhou is now working as a full-time research staff in Institute of Chemical Materials, China Academy of Engineering Physics. He received his B.S. degree and M.S. degree from Tianjin University in 2014 and 2017, respectively. His current research focuses on design and fabrication of novel multi-functional nanostructures and their applications on fiber-shaped energy storage system.

Wei Ni received his B.S. degree in Polymer Materials and Engineering from Zhengzhou University in 2005 and Ph.D. degree in Chemistry from Institute of Chemistry, Chinese Academy of Sciences in 2011. He is currently a research associate at Institute of Chemical Materials, China Academy of Engineering Physics. His current research interests involve nanostructured composite materials for energy and environment related applications.

Bin Wang is a staff scientist in the National Energy Novel Materials Center (NENMC, China), and Institute of Chemical Materials, China Academy of Engineering Physics (ICM-CAEP). He received his Ph.D. degree from Fudan University in 2009. He was a postdoctoral scholar at Lawrence Berkeley National Lab (LBNL, USA) during 2009–2013 and then joined the NENMC and ICM-CAEP. He published over 52 peer-reviewed papers in professional journals. His research focuses on development and applications of novel materials for energy conversion and storage. He has been awarded excellent contribution honor in 17th IUPAC FCFP- XVII & NMS-III.

Sisi He received her Ph.D. in 2017 at Macromolecular Chemistry and Physics at Fudan University, BS in Material Science and Engineering from Northeastern University in 2011, and MS in Material Science and Engineering from Tianjin University in 2014. Her work focuses on the development of flexible and wearable actuators, sensors, energy storage device, electricity generator and biocompatible material, from controlled growth and properties tunable super aligned carbon nanotube assembly.

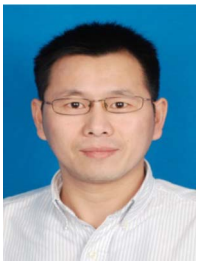

Huisheng Peng received his Ph.D. in Chemical Engineering from Tulane University in USA in 2006. He worked at Los Alamos National Laboratory, US Department of Energy, from 2006 to 2008. Dr. Peng has been appointed as a Professor at the Department of Macromolecular Science and Laboratory of Advanced Materials at Fudan University since October 2008. He served as an Associate Chair at Department of Macromolecular Science since 2012 and Director of the Center of Polymers and Their Advanced Composite Materials since 2014. His research focuses on the development of novel energy materials and devices particularly based on polymers.